

## Temperature dependent work hardening in Ti–6Al–4V alloy over large temperature and strain rate ranges: Experiments and constitutive modeling



Guang Chen <sup>a,\*</sup>, Chengzu Ren <sup>b,\*</sup>, Xuda Qin <sup>a</sup>, Jun Li <sup>a</sup>

<sup>a</sup> Key Laboratory of Equipment Design and Manufacturing Technology, Tianjin University, Tianjin 300072, China

<sup>b</sup> Key Laboratory of Advanced Ceramics and Machining Technology of Ministry of Education, Tianjin University, Tianjin 300072, China

### ARTICLE INFO

#### Article history:

Received 12 March 2015

Revised 17 May 2015

Accepted 7 June 2015

Available online 19 June 2015

#### Keywords:

Ti–6Al–4V alloy

Constitutive behavior

Work hardening

Deformation mechanisms

Flow stress

### ABSTRACT

The plastic deformation behaviors of Ti–6Al–4V alloy over wide ranges of strain rate (from  $10^{-4}$  to  $10^4 \text{ s}^{-1}$ ) and temperature (from 20 to 900 °C) are investigated by the quasi-static and dynamic uniaxial compression tests. The microstructure evolution of Ti–6Al–4V alloy at different temperatures is discussed. Material generates higher ductility and formability when temperature is higher than 500 °C, which leads to the decrease of work hardening rate. The true stress–strain responses are modeled with the JC, modified JC, KHL and modified KHL models. In detail, a temperature dependent work hardening function is introduced into the original JC and KHL models. The parameters of the four models for Ti–6Al–4V alloy are calculated by GA optimization method. The average standard deviations between the experimental and calculated flow stresses range from 4% to 13%, which validates the accuracy of the models. In addition, comparison of flow stresses at dynamic ( $10,000 \text{ s}^{-1}$ ), the work hardening rates at dynamic ( $7500 \text{ s}^{-1}$ ), as well as the quasi-static jump experiments were proposed to further validate the models. The modified JC and modified KHL models could characterize the temperature dependent work hardening effect for Ti–6Al–4V alloy over large strain rate and temperature ranges.

© 2015 Elsevier Ltd. All rights reserved.

## 1. Introduction

For more than fifty years, titanium and its alloys have been introduced in aerospace, energy and chemical industry. They have less density and high mechanical strength to weight, good corrosion resistance, and these properties make them behave excellent as blade of aviation engines, gas turbine engines and airframe [1,2]. Ti–6Al–4V alloy, a typical  $\alpha + \beta$  titanium alloy, due to its good combined thermal and mechanical behavior, has been widely used in aerospace, chemical pressure vessels, medical surgical implant, military armor [3], etc. Normally, the manufacture of components, for example, forging, punching and cutting, has specific precise requirements on mechanical and physical properties [4,5]. Dynamic deformation behavior of titanium alloys is very important not only in impact and penetration related problems [6–8], but also for the high speed machining and the accompanied shear deformation behavior [9–12].

According to previous quasi-static and dynamic loading data, several constitutive models have been proposed to characterize

the visco-plastic deformation responses of metals. These models can be broadly classified as two main groups: the phenomenological models and the physical based models. The phenomenological models which are commonly calculated according to the flow stress responses, for example, the models proposed by Johnson and Cook [13], Seo et al. [14], Sung et al. [15], Steglich et al. [16], and the KHL models [17,18], etc. While, the physical based models [19–22] were commonly developed involving the physical state of the materials (e.g. grain size, dislocation density, etc.).

Although the physical-based models are often linked to microscopic deformation quantities that provide the potential understanding of plastic deformation, both phenomenological and physical-based models use macroscopic uniaxial loading responses to determine the material constants. The superiority of one model over the other should consider the number of the material constants in each model, and from mathematical formulas, any model with a large number of material parameters is supposed to approximate the test responses primarily [17,23].

Mecking and Kocks [24] proposed an approach to predict the variation of dislocation energy for stage III hardening of materials, and the developed constitutive model was applied using 23 constants [25]. Based on the Mecking–Kocks model, Luo et al. [26]

\* Corresponding authors.

E-mail addresses: [guangchen@tju.edu.cn](mailto:guangchen@tju.edu.cn) (G. Chen), [renchz@tju.edu.cn](mailto:renchz@tju.edu.cn) (C. Ren).

developed a constitutive model considering grain size and dislocation energy, according to the compression tests at temperatures ranging from 1093 to 1303 K and the strain rates ranging from 0.001 to  $10\text{ s}^{-1}$ . The model consists of 20 constants that were identified by the isothermal flow stresses and grain size of prior  $\alpha$  phase. Babu and Lindgren [5] presented a constitutive model for Ti-6Al-4V alloy based on the evolution of immobile dislocation density and excess vacancy concentration. There are 12 temperature dependent constants in the model, which were calibrated by compression tests at each temperature condition, from 20 °C to 1100 °C, that is, a large number of constants are needed to characterize the flow stresses for different loading conditions. The constitutive models with large number of constants may be useful to improve the prediction accuracy, but it is not easy to obtain the values, and also, it is difficult to be widely applied in the modeling of machining process. Nemat-Nasser et al. [3] developed a concise physical based model that consisted of 8 constants, which were determined by the compression tests of Ti-64 alloy, considering the effect of strain aging. Although some models with fewer constants, for example, the Johnson and Cook (J-C) model and Khan-Huang-Liang (KHL) model, have 5 or 6 constants, they can also give high accurate prediction of flow stresses [14,27]. With identical prediction accuracy, models with less constants are easier to be applied in modeling of the machining process, for example, the J-C model has been widely utilized in numerical modeling for material forming, especially in large deformation machining, i.e., metal cutting.

For Ti-6Al-4V alloy, the uniaxial load tests can be mainly classified in two categories according to the loading condition: one kind is carried out with low strain rate and high temperature [28,29], which aims to develop material constitutive models for the hot forming manufacturing, involving hot forming, forging, welding, etc. In hot working, deformation commonly involves the changes of the physical state of materials (e.g. dynamic recrystallization, phase transformation, and dislocation, etc.); The other was commonly proposed with high strain rate and relatively low temperature [3,6,18], focusing on the deformation and material removal in machining, involving cutting, milling and drilling, etc.

Material plastic deformation commonly behaves coupled effects of work hardening, thermal softening and strain rate hardening in terms of the interrelationship of stress, strain, strain rate and temperature. Some models have been presented to characterize the negative strain rate sensitivity (SRS) [30–32] and negative to positive coupled SRS [33] phenomena in material deformation. Meanwhile, some researches focused on the working hardening rate of the materials. Khan et al. [7] proposed a modified KHL model to correlate the decreasing work hardening rate with increase in strain rate and strain in responses of Ti-6Al-4V compression tests. Besides, the grain size and temperature effect were introduced to the KLF model to describe the work hardening behavior of milled Cu [34]. In addition, according to the Ti-6Al-4V compression test, the work hardening behavior exhibited close relationship with temperature [5]. Over all, to obtain an accurate constitutive model, the material plastic deformation should consider the coupled effects of the strain, strain rate and temperature.

The main objective of this work is to investigate the material deformation behavior at a wide range of temperatures (20–900 °C) and strain rates ( $10^{-4}$ – $10^4\text{ s}^{-1}$ ), which may cover the machining and hot working processes for Ti-6Al-4V alloy. In this work, the J-C and KHL models are utilized to model the flow stresses for Ti-6Al-4V alloy. In addition, the flow stresses exhibit a temperature dependent strain (or work) hardening behavior, then two modified JCM and KHL models considering temperature dependent hardening behavior were proposed to characterize the flow stresses under wide ranges of strain rate and temperature.

## 2. Experimental procedure and results

### 2.1. Material and experiments

Ti-6Al-4V alloy is a two-phase alloy containing about 6 wt% Al and 4 wt% V, which stabilize the hexagonal close packed (HCP) structure, named  $\alpha$  phase and body-centered cubic (FCC) structure, named  $\beta$  phase, respectively. The two phases have different properties due to their structures. Compared with  $\beta$  phase,  $\alpha$  exhibits higher resistance to plastic deformation but lower ductility and formability [35]. Generally, the microstructures of Ti-6Al-4V is affected by the thermo-mechanical treatment, and the key point for thermo-mechanical treatment is the  $\beta$ -transition temperature, above which the  $\alpha$  phase transforms to  $\beta$ . For titanium alloy, this temperature depends on the composition of Al and V. The  $\beta$ -transition temperature for Ti-6Al-4V is approximately 1010 °C [36].

In this study, a commercial grade titanium alloy (Ti-6Al-4V) plate with thickness of 10 mm was used to fabricate the cylindrical specimens. This Ti-6Al-4V alloy has lamellar starting structure which is shown in Fig. 1, and the chemical composition of the alloy is listed in Table 1. The similar lamellar microstructure titanium alloy has been used in different researches in order to investigate the plastic deformation behaviors in hot working and machining [36,37]. The cylindrical specimens machined from the plate were used in the uniaxial compression tests, and the axis of the specimens is oriented in the transverse direction (TD) of rolling.

### 2.2. Quasi-static and dynamic compression tests

In this work, the uniaxial compression tests of Ti-6Al-4V alloy were conducted in the strain rate range  $10^{-4}$ – $10^4\text{ s}^{-1}$  with two different test systems. The quasi-static compression tests were performed at the strain rates of  $0.0001\text{ s}^{-1}$  and  $0.01\text{ s}^{-1}$  on a DNS100 test machine, which has a load capacity of 100 kN. The specimens of the quasi-static tests were machined with 5 mm diameter and 4 mm length. All of the specimens were machined by wire electro-discharge machining (WEDM) from the titanium alloy plates.

The dynamic tests were performed at strain rates of  $2500\text{ s}^{-1}$ ,  $4000\text{ s}^{-1}$ ,  $7500\text{ s}^{-1}$  and  $10,000\text{ s}^{-1}$ , and a wide range of temperatures, 20 °C, 100 °C, 300 °C, 500 °C, 700 °C and 900 °C, using the enhanced Hopkinson technique [38]. The schematic of the split Hopkinson bar system is shown in Fig. 2. According to the one dimensional stress propagation theory, the average strain, stress, and strain rate can be calculated by the measured incident, reflected and transmitted pulses,  $\varepsilon_i$ ,  $\varepsilon_r$  and  $\dot{\varepsilon}_t$ , respectively, according to the following equations [22]:

$$\varepsilon_s(t) = -\frac{2c_0}{l_s} \int_0^t \varepsilon_R(t) dt \quad (1)$$

$$\sigma_s = \frac{A_b E_b \varepsilon_t}{A_s} \quad (2)$$

$$\dot{\varepsilon}_s = -\frac{2c_0 \varepsilon_R}{l_s} \quad (3)$$

where  $c_0$  is the wave speed in the bar,  $E_b$  and  $A_b$  are the Young's modulus and the cross-sectional area of the pressure bars.  $A_s$  and  $l_s$  are the cross-sectional area and the length of the cylindrical specimen.  $\sigma_s$ ,  $\varepsilon_s$  and  $\dot{\varepsilon}_s$  are the stress, strain and strain rate in the specimen.

The specimens of the dynamic test were machined with 2 mm diameter and 1.8 mm length by WEDM processing. During the tests, the temperature of the specimen was measured by thermocouple technology. In addition, to avoid temperature gradient

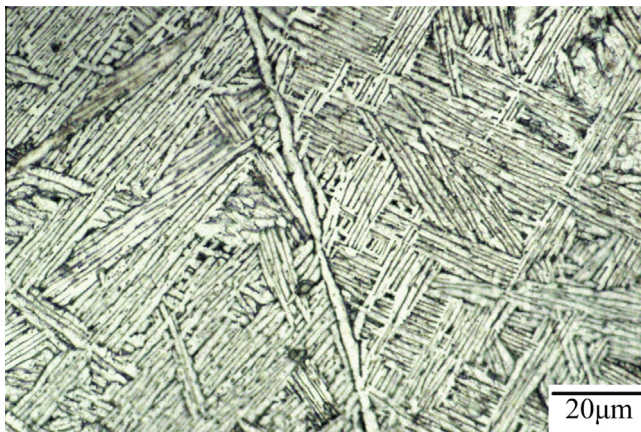


**Fig. 1.** The microstructure of Ti-6Al-4V used in this investigation.

which may change the elastic constants of the incident and transmit bars, the specimen needs to be heated to the required temperature while keeping the incident and transmit bars of the Hopkinson device at suitable low temperature [39]. The temperature of specimen was kept approximately constant within  $\pm 3$  °C in 10 min, using the electro-thermal cells, to avoid heat treatment effect on the specimen. The metallographic and temperature effects induced from the WEDM of the new specimen are neglected here.

In this work, all the experimental data were converted to true stress  $\sigma$  and true strain  $\varepsilon$  curves. The plastic strain  $\varepsilon_p$  was determined by  $\varepsilon_p = \varepsilon - \sigma/E - 0.002$ , the yield strength was determined by 0.2% offset yield stress in the stress-strain curves [40].

In addition, the temperature increase subjected to adiabatic process in dynamic loading is determined by the following equations [41],

$$\Delta T = \frac{0.95\eta}{\rho C_p} \int_0^{\varepsilon} \sigma d\varepsilon \quad (4)$$

where  $\rho$  is the density of the material,  $C_p$  is the specific heat, and  $\eta$  is the thermal efficiency that is calculated as following [42],

$$\eta = \begin{cases} 0 & \dot{\varepsilon} \leq 10^{-3} \text{ s}^{-1} \\ 0.316 \lg \dot{\varepsilon} + 0.95 & 10^{-3} \text{ s}^{-1} < \dot{\varepsilon} < 1.0 \text{ s}^{-1} \\ 0.95 & \dot{\varepsilon} \geq 1.0 \text{ s}^{-1} \end{cases} \quad (5)$$

In this work, the density of Ti-6Al-4V alloy,  $\rho$  is 4430 kg/m<sup>3</sup>; the value of  $C_p$  is specified according to the function of the temperature [43].

$$C_p = 559.77 - 0.1473T + 0.00042949T^2 \text{ J/(kg K)} \quad (278 \text{ K} < T < 1144 \text{ K}) \quad (6)$$

In addition, the specific heat of the highest temperature 900 °C in the dynamic test was estimated approximately, using the limitation temperature of Eq. (6), 871 °C (1144 K). Thus, the calculated temperature increase of the experimental results is utilized when modeling the flow stresses.

### 2.3. Temperature dependent effect

The work (or strain) hardening effect is commonly related with the strain rate condition, for some kinds of material, it shows low dependence on the temperature [40]. In this work, to investigate the work hardening rate at different temperature conditions, the work hardening rate  $Q$  was determined according to the measured changing rate of the stress, i.e., the slope of the stress-strain curve at specific strain

$$Q = \frac{\delta\sigma}{\delta\varepsilon} = \frac{\sigma_i - \sigma_{i-1}}{\varepsilon_i - \varepsilon_{i-1}}, \quad i \geq 1 \quad (7)$$

where  $i$  is the number of the points measured in the tests. The calculated work hardening rate is shown in Fig. 3. At low strain condition, the hardening rate decreases rapidly with the increase of strain. Afterwards, the hardening rate decreases slightly until it reaches a stable value. Under quasi-static condition ( $0.01 \text{ s}^{-1}$ ), the hardening rate exhibits a smoothly decreasing trend; in addition, it is dependent on the temperature. That is, the hardening rate decreases with the increase of the temperature (from 20 °C to 700 °C). Under the dynamic loading condition ( $2500 \text{ s}^{-1}$ ,  $4000 \text{ s}^{-1}$ ,  $7500 \text{ s}^{-1}$ ,  $10,000 \text{ s}^{-1}$ ), it exhibits a fluctuated decreasing trend, which is caused by the fluctuation of the measured flow stresses. According to the one dimensional stress propagation theory, substituted the strain and stress definition Eqs. (1) and (2) in Eq. (7), the work hardening rate can be defined as

$$Q = -\frac{A_b E_b l_s [\varepsilon_T(t_i) - \varepsilon_T(t_{i-1})]}{2c_0 A_s \left( \int_0^{t_i} \varepsilon_R dt - \int_0^{t_{i-1}} \varepsilon_R dt \right)} \quad (8)$$

that is, the fluctuation of work hardening rate is related with the transmitted pulse and the integrated reflected pulse, and this phenomenon commonly exists for high strain rate SHPB tests [14,40]. The hardening rate at 20 °C is obviously higher than those at 700 °C and 900 °C, especially for high strain rate conditions. For instance, the hardening rates at 7500 and  $10,000 \text{ s}^{-1}$  decrease with the increase of temperature more obviously than other conditions, as shown in Fig. 3d and e. Over all, considering the fluctuation of flow stresses at the SHPB tests, the flow stresses of Ti-6Al-4V alloy exhibit temperature dependent work hardening effect, and work hardening rates decrease gradually with the increase of the temperature, which is more obviously for high strain rate conditions.

### 2.4. Temperature dependent microstructure

To study the temperature effect on deformation process, the specimens and their microstructure after deformation at  $10,000 \text{ s}^{-1}$  were observed using the KEYENCE® VHX-1000 microscope and a scanning electron microscope (SEM). The samples were sectioned along the loading axis, polished with abrasive papers, and then were etched in a solution of 3 ml HF, 5 ml HNO<sub>3</sub> and 100 ml H<sub>2</sub>O, for ~3 min until the microstructure was revealed.

The deformed specimens and microstructure (in selected rectangle area) at  $10,000 \text{ s}^{-1}$ , 20–900 °C are shown in Fig. 4a-f. In addition, the cross-section geometry of the deformed specimen and the loading direction are illustrated in Fig. 4a. At 20 °C, 100 °C and 300 °C, specimen generates shear band and crack that was normally formed along a 45° loading axis. When temperature is lower

**Table 1**  
Chemical composition of commercial Ti-6Al-4V alloy.

Element	Ti	Al	V	Fe	C	N	H	O
Percent weight composition	Bal.	5.5–6.75	3.5–4.5	<0.3	<0.08	<0.05	<0.015	<0.2

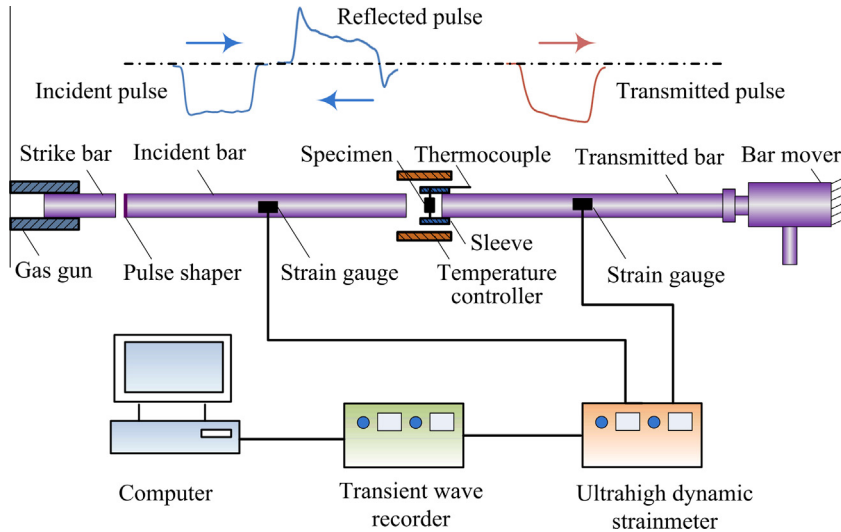


**Fig. 2.** The schematic of the split Hopkinson bar system.

than 500 °C, the microstructure of the specimen is typical lamellar microstructure with light small beam  $\beta$  around the coarse gray  $\alpha$  phase. At higher temperature (500 °C, 700 °C and 900 °C), specimen generates larger plastic deformation and no obvious crack formed, except for a small area at 500 °C. Within the scope of hot working, from 600 °C to 995 °C, part of  $\alpha$  phase will transform into  $\beta$ , and the volume fraction of  $\beta$  phase increases with deformation temperature when the cooling strategy is identical [44,45]. More  $\beta$  phase will lead to higher ductility and formability, for example, specimen generates larger plastic deformation at 500 °C, 700 °C and 900 °C (as shown in Fig. 4d–f), especially for the highest temperature condition. Micro-mechanism like dynamic recovery, dynamic recrystallization and grain boundary sliding can also be considered as a function of  $\beta$  phase fraction in titanium alloy [46]. Normally, the grain boundary sliding occurs at high temperature and low strain rate conditions. For high strain rate SHPB tests, the behavior of dislocation annihilation that can be driven by dynamic recrystallization and dynamic recovery will cause higher ductility and the decrease of work hardening rate. At 500 °C and 700 °C conditions, the specimens generate strain localization along a white adiabatic shear band (ASB), and recrystallization may exist in the middle of ASB [44]. Schneider et al. [47] estimated the critical temperature of ASB formation is 773 K (500 °C) as 0.4 times of the absolute melting temperature 1933 K (1660 °C for Ti-6Al-4V), and the recrystallization was not fully driven when the estimated temperature is lower than the critical temperature. Besides, compared with the lower temperature conditions, the microstructure outside of the ASB is also changed. At 900 °C, specimen generates severe plastic deformation instead of the narrow ASB, meanwhile, the microstructure exhibits smaller grain size than other conditions. Normally, the compression tests conducted below 500 °C show little rate dependence and generate hardening effect followed by fracture (or crack); while tests between 500 °C and 700 °C will result in flow softening or hardening decreasing after the initial hardening [5]. Overall, 500 °C can be approximately considered as the critical temperature for Ti-6Al-4V alloy deformation and microstructure evolution mechanism, and also can be regarded as the threshold temperature for its deformation involves machining and hot working.

### 3. Constitutive modeling

The constitutive model of material plastic deformation is normally a function of the strain, strain rate and temperature. Some

constitutive models have been developed to characterize the behaviors of work hardening, strain-rate hardening, thermal softening and the coupled effect of materials caused by impact loading. A simple constitutive expression of the flow stress for material in plastic deformation can be given as follows

$$\sigma = f(\varepsilon, \dot{\varepsilon}, T) \quad (9)$$

the work hardening rate  $Q$ , strain rate hardening rate  $R$  and thermal softening rate  $P$  can be defined as

$$Q = \frac{\delta\sigma}{\delta\varepsilon}, \quad R = \frac{\delta\sigma}{\delta\dot{\varepsilon}}, \quad P = \frac{\delta\sigma}{\delta T} \quad (10)$$

In this work, the JC and KHL constitutive models are applied to model the flow stresses of Ti-6Al-4V alloy at the wide ranges of strain rate and temperature. Besides, the two models are modified to concern the temperature dependent work hardening effect. Then, these models are addressed in the following sections and the parameters of the models are determined directly for each model.

#### 3.1. The Johnson Cook (JC) model

The JC model [13] is a widely used constitutive model for thermo-mechanical deformation processes, and the equivalent flow stress is defined as

$$\sigma = [A + B(\varepsilon)^n] \left[ 1 + C \ln \left( \frac{\dot{\varepsilon}}{\dot{\varepsilon}_0} \right) \right] \left[ 1 - \left( \frac{T - T_r}{T_m - T_r} \right)^m \right] \quad (11)$$

where  $\varepsilon$ ,  $\dot{\varepsilon}$  and  $\dot{\varepsilon}_0$  are the plastic strain, plastic strain rate and reference strain rate, in this part, the reference strain rate is defined as  $\dot{\varepsilon}_0 = 0.01 \text{ s}^{-1}$ .  $A$ ,  $B$ ,  $n$ ,  $C$  and  $m$  are material parameters, and  $T_r$  (20 °C) and  $T_m$  (1660 °C) are the reference ambient temperature and melting temperature of Ti-6Al-4V alloy, respectively.

To obtain the material parameters for the compression test conditions, a genetic algorithm (GA) optimization method [48] is utilized to optimize the parameters by minimizing the relative errors of the measured flow stress and the calculated flow stress by JC model. Normally, the initial values input into the optimization procedure can be determined by given experimental flow stresses [34]. The initial values to be implemented into the optimized subroutine are defined as following.

The parameter  $A$  can be determined at the reference condition ( $T = T_r$ ,  $\dot{\varepsilon}_0 = 0.01 \text{ s}^{-1}$ ). That is,  $A$  equals to the stress when  $\varepsilon = 0$ . At reference condition, the JC model can be transformed to

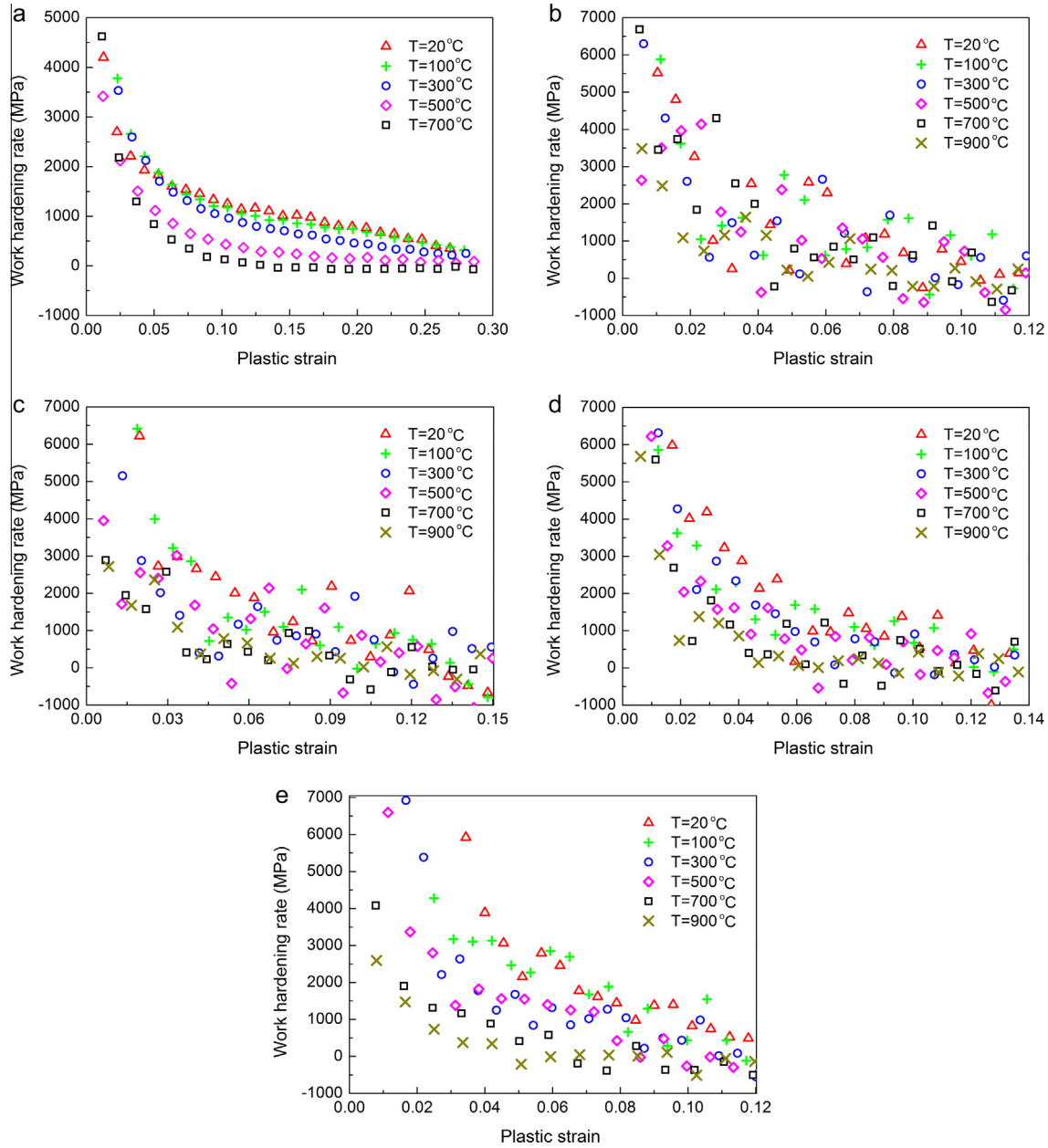


**Fig. 3.** The work hardening rate of the Ti-6Al-4V alloy at different temperatures for the strain rate of (a)  $0.01 \text{ s}^{-1}$ , (b)  $2500 \text{ s}^{-1}$ , (c)  $4000 \text{ s}^{-1}$ , (d)  $7500 \text{ s}^{-1}$  and (e)  $10,000 \text{ s}^{-1}$ .

$$\sigma = A + B(\varepsilon)^n \quad (12)$$

$$\ln(\sigma - A) = n \ln \varepsilon + \ln B \quad (13)$$

Then, the parameters  $A$ ,  $B$  and  $n$  can be obtained by fitting the curve of  $\ln(\sigma - A)$  vs.  $\ln \varepsilon$  at the reference condition. The parameter  $C$  can be obtained at the specific temperature and strain condition ( $T = T_r$ ,  $\varepsilon = 0.1$ ), and the JC model can be simplified as

$$\sigma = [A + B(\varepsilon)^n] \left[ 1 + C \ln \left( \frac{\dot{\varepsilon}}{\dot{\varepsilon}_0} \right) \right] \quad (14)$$

$$\frac{\sigma}{A + B(\varepsilon)^n} - 1 = C \ln \left( \frac{\dot{\varepsilon}}{\dot{\varepsilon}_0} \right) \quad (15)$$

Using the obtained constants  $A$ ,  $B$  and  $n$ , the parameter  $C$  is determined as the slope of the fitting curve of  $[\sigma/(A + B(\varepsilon)^n) - 1]$  vs.  $\ln(\dot{\varepsilon}/\dot{\varepsilon}_0)$ . The last step is to calculate the parameter  $m$  with given

data of flow curve, for example, at a specific strain (0.1) and at a particular strain rate ( $2500 \text{ s}^{-1}$ ),  $m$  can be determined as the slope of the following response

$$\ln \left( 1 - \frac{\sigma}{[A + B(\varepsilon)^n] \left[ 1 + C \ln \left( \frac{\dot{\varepsilon}}{\dot{\varepsilon}_0} \right) \right]} \right) = m \ln \left( \frac{T - T_r}{T_m - T_r} \right) \quad (16)$$

Thus, the JC parameters are evaluated in terms of the limited flow stresses. It should be noted that, the material parameters ( $A$ ,  $B$ ,  $n$ ,  $C$  and  $m$ ) obtained by the proposed procedure are not the final constants which can describe the flow stresses accurately, because the parameters are calculated according to the limited experimental points. Therefore, they are adopted as the initial values for the optimization procedure. After the optimization, the initial and optimized results are presented in Table 2. Meanwhile, the comparison of predicted and measured flow stresses (dash line and symbols) is shown in Fig. 5. The predicted flow stresses agree well

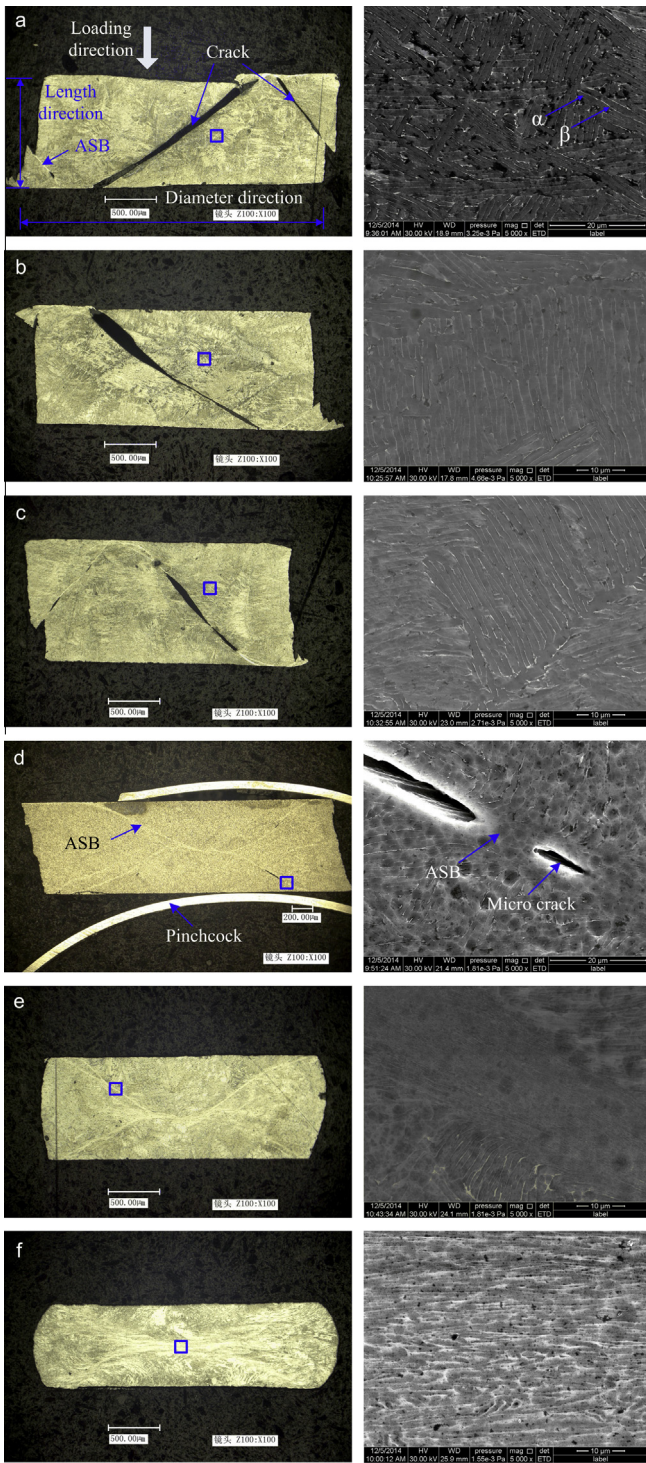


**Fig. 4.** Deformed specimens and the microstructure at  $10,000\text{ s}^{-1}$  and different temperatures (a)  $20\text{ }^{\circ}\text{C}$ , (b)  $100\text{ }^{\circ}\text{C}$ , (c)  $300\text{ }^{\circ}\text{C}$ , (d)  $500\text{ }^{\circ}\text{C}$ , (e)  $700\text{ }^{\circ}\text{C}$  and (f)  $900\text{ }^{\circ}\text{C}$ .

with the experimental results for most curves. However, as shown in Fig. 5c-f, some larger relative errors exist at high temperature ( $T > 500\text{ }^{\circ}\text{C}$ ) since the predicted work hardening effect is larger than that of experiments, especially for high strain rate conditions.

### 3.2. The modified Johnson Cook (JCM) model

As discussed in Section 2.3, the work hardening rate exhibits temperature dependence. For example, at the dynamic loading

conditions ( $2500\text{ s}^{-1}$ ,  $4000\text{ s}^{-1}$ ,  $7500\text{ s}^{-1}$ ,  $10,000\text{ s}^{-1}$  as shown in Fig. 3), the hardening rate becomes smaller when the temperature is above  $500\text{ }^{\circ}\text{C}$ , and it exhibits a decreasing trend with the increase of temperature. At the quasi-static condition ( $0.01\text{ s}^{-1}$ ), when the temperature is lower than  $500\text{ }^{\circ}\text{C}$  the hardening rate is also decreasing with the increase of temperature, as shown in Fig. 3a. In addition, the temperature dependent work hardening effect can be observed from the comparison of the measured flow stresses and the JC model predicted flow stresses. For instance, the hardening rate of calculated flow stresses by JC model is lower than the experimental results when  $T < 500\text{ }^{\circ}\text{C}$ , whereas it is larger than the experimental results when  $T > 500\text{ }^{\circ}\text{C}$ , as shown in Fig. 5b. According to the microstructure observation of  $10,000\text{ s}^{-1}$ ,  $500\text{ }^{\circ}\text{C}$  can be approximately considered as the critical temperature for Ti-6Al-4V compression tests. Above it, material exhibits higher ductility and formability, which will decrease the work hardening rate.

In order to characterize this temperature dependent hardening effect, a temperature function  $\varphi(T)$  was introduced into the work hardening term in JC model.

$$\varphi(T) = \frac{T_0 - T}{T_0} \quad 450 < T_0 < 700\text{ }^{\circ}\text{C}, \quad 0 < T < 1000\text{ }^{\circ}\text{C} \quad (17)$$

The domains of constant  $T_0$  and  $T$  are related with the temperature range of the compression tests, in this work, they are defined as  $450 < T_0 < 700\text{ }^{\circ}\text{C}$ ,  $0 < T < 1000\text{ }^{\circ}\text{C}$ . In addition, to make the temperature term of work hardening rate has a property scope (between 0 and 1) for adjusting the temperature effect, an exponential function  $\phi(T)$  was specified as

$$\phi(T) = \left[ \frac{1 + \varphi(T)}{2} \right]^{n_2} = \left( \frac{T_0 - T/2}{T_0} \right)^{n_2} \quad (18)$$

where  $n_2$  ( $0 < n_2 < 1$ ) is an exponential coefficient. When the temperature  $T$  increases, the value of the temperature dependent hardening rate term  $\phi(T)$  lies between 0 and 1. This part is added into the JC model to adjust the work hardening effect at different temperatures, thus the modified JC (JCM) model is defined as

$$\sigma = \left[ A + B \left( \frac{T_0 - T/2}{T_0} \right)^{n_2} (\dot{\varepsilon})^n \right] \left[ 1 + C \ln \left( \frac{\dot{\varepsilon}}{\dot{\varepsilon}_0} \right) \right] \left[ 1 - \left( \frac{T - T_r}{T_m - T_r} \right)^m \right] \quad (19)$$

In this part, the similar method is applied to calculate the initial values for the parameters. To calculate parameter  $n$ , the initial value of  $T_0$  is specified as  $500\text{ }^{\circ}\text{C}$  according to the results of work hardening and microstructure evolution. Firstly, a temperature dependent parameter  $K$  is given as

$$K = B \left( \frac{T_0 - T/2}{T_0} \right)^{n_2} \quad (20)$$

$A$  is determined at the reference condition ( $T = T_r$ ,  $\dot{\varepsilon} = 0.01\text{ s}^{-1}$ ), meanwhile, as  $B$  and  $n_2$  are constants,  $K$  can be considered as a constant at the condition of  $T = T_r$ ,  $\dot{\varepsilon} = 0.01\text{ s}^{-1}$ , the constitutive equation is simplified as

$$\sigma = A + K(\dot{\varepsilon})^n \quad (21)$$

$$\ln(\sigma - A) = n \ln \dot{\varepsilon} + \ln K \quad (22)$$

therefore,  $n$  is obtained by fitting the slope of  $\ln(\sigma - A)$  vs.  $\ln \dot{\varepsilon}$  at the reference condition. Then parameters  $A$ ,  $n$  and  $K$  can be obtained. Afterwards, the parameter  $C$  can be obtained at given temperature, strain (e.g.  $T = T_r$ ,  $\dot{\varepsilon} = 0.1$ ) and different strain rates, by fitting the slope of the curve of  $[\sigma/(A + K(\dot{\varepsilon})^n) - 1]$  vs.  $\ln(\dot{\varepsilon}/\dot{\varepsilon}_0)$ .

$$\frac{\sigma}{A + K(\dot{\varepsilon})^n} - 1 = C \ln \left( \frac{\dot{\varepsilon}}{\dot{\varepsilon}_0} \right) \quad (23)$$

Because the calculated methods of  $A$ ,  $n$  and  $C$  are identical with original JC model, the calculated initial values are same as the parameters in Table 2. Afterwards, the constants  $B$ ,  $m$  and  $n_2$  need to be determined. As the constants  $B$  and  $n_2$  are temperature dependent hardening coefficients, and  $m$  is the coefficient of the thermal softening, they will affect with each other in the temperature dependent model. As a result, it is difficult to fit these constants by some given flow stress independently. Concerning the temperature dependent strain hardening effect (Fig. 3), some flow stresses with obvious temperature dependent hardening effect are adopted to calculate the initial values of the constants. The flow stresses under different temperatures, at  $\dot{\varepsilon} = 10,000 \text{ s}^{-1}$  and  $\varepsilon = 0.05$ , are applied into the GA optimization to calculate the constants  $B$ ,  $m$  and  $n_2$ , aiming to minimize the relative errors of the predicted and measured flow stresses. The calculated initial values of  $B$ ,  $m$  and  $n_2$  are listed in Table 3. Ultimately, the initial values of the constants are input into the GA optimization procedure, and the parameters of the JCM model are optimized, as listed in Table 3, by minimizing the errors between the predicted and the measured flow stresses for the 30 loading conditions, covering the wide ranges of strain rate and temperature. The predicted flow stresses by JCM model (solid lines) are also shown in Fig. 5. The predicted flow stresses agree very well with the measured flow stresses over the entire ranges of strain rate and temperature. Compared with the JC model, the predicted results of JCM model are closer to experimental results due to the smaller work hardening rate at high temperature ( $T > 500^\circ\text{C}$ ) conditions. In addition, it should be noted that at the highest temperature and high strain rate conditions, for example, at  $900^\circ\text{C}$  and  $4000 \text{ s}^{-1}$ , as shown in Fig. 5d, the flow stress even generates the strain softening effect, i.e., the stress decreases slightly with the increasing strain, which is caused by adiabatic temperature rise with the increase of the plastic strain.

### 3.3. The Khan–Huang–Liang (KHL) constitutive model

In this research, the KHL constitutive model, which has been used to successfully predict the thermo-mechanical behavior of different materials [7,18,40], is used to model the compression test responses. The KHL plastic constitutive model and the equivalent stress is defined as

$$\sigma = \left[ A + B \left( 1 - \frac{\ln \dot{\varepsilon}}{\ln D_0} \right)^{n_1} \varepsilon^{n_0} \right] \left( \frac{\dot{\varepsilon}}{\dot{\varepsilon}_0} \right)^C \left( \frac{T_m - T}{T_m - T_r} \right)^m \quad (24)$$

where  $D_0 = 10^6 \text{ s}^{-1}$  is a constant that is used to non-dimensionalize the strain rate term.  $A$ ,  $B$ ,  $n_1$ ,  $n_0$ ,  $C$  and  $m$  are six material parameters of the KHL constitutive model. The GA optimization method was also performed to get these parameters. In the former JC and JCM optimization, calculation results exhibit that the initial values have little influence on calculation results when the value ranges of material parameters are provided. In this section, to minimize the relative errors between the entire ranges of the predicted and experimental flow stresses, the GA optimization was carried out without the calculated initial value as JC and JCM model. The optimization procedure is considered as a mathematical problem, which is aiming to minimize the relative errors of the predicted and measured flow curves at the 30 conditions, and the reference strain rate is given as  $\dot{\varepsilon}_0 = 1 \text{ s}^{-1}$ , referring to the former KHL modeling work [7,18]. The optimized results are shown in Table 4. The constant  $n_1$  equals to zero, which indicates that the strain rate has little influence on the work hardening at the wide ranges of strain rate and temperature for this model.

Using the KHL model and the optimized parameters, the comparison of measured and calculated flow stresses (symbols and dash lines) are shown in Fig. 6. The predicted flow stresses are

consistent with the measured flow stresses over the wide range conditions.

### 3.4. The modified KHL (KHLM) model

Although good agreement is achieved by the KHL model, the work hardening rate of the predicted flow stress for high temperature is still larger than the experimental results. That is, the KHL model cannot characterize the temperature effect effectively. For instance, when the temperature is larger than  $500^\circ\text{C}$ , the hardening rates of the measured flow curves are smaller than the KHL predicted curve. At the quasi-static condition (Fig. 6b)  $100^\circ\text{C}$  and  $300^\circ\text{C}$ , the hardening rate is also decreasing with the increase of temperature, and the hardening rate of the measured curves are slightly larger than that of KHL predicted flow curves.

To characterize the decreasing work hardening with the increasing temperature, the temperature dependent work hardening function is also added into the KHL model, thus the KHLM model is given by

$$\sigma = \left[ A + B \left( 1 - \frac{\ln \dot{\varepsilon}}{\ln D_0} \right)^{n_1} \left( \frac{T_0 - T/2}{T_0} \right)^{n_2} \varepsilon^{n_0} \right] \left( \frac{\dot{\varepsilon}}{\dot{\varepsilon}_0} \right)^C \left( \frac{T_m - T}{T_m - T_r} \right)^m \quad (25)$$

where  $450 < T_0 < 700^\circ\text{C}$ , the reference strain rate is defined as  $\dot{\varepsilon}_0 = 1 \text{ s}^{-1}$ , and the constant  $D_0 = 10^6 \text{ s}^{-1}$ .  $A$ ,  $B$ ,  $n_1$ ,  $n_2$ ,  $n_0$ ,  $C$  and  $m$  are the parameters of the KHLM constitutive model. Using the GA optimization method, the optimized results are listed in Table 5. The predicted flow stresses by KHLM model (solid lines) are also shown in Fig. 6. Compared with KHL model, the predicted results of KHLM model describes the work hardening effect more accurately at  $700^\circ\text{C}$  and  $900^\circ\text{C}$ . For other conditions, both of the KHL and KHLM models agree with the experiments well.

## 4. Verification and comparison of constitutive models

In this work, the four constitutive models are developed and the parameters for Ti–6Al–4V alloy are obtained by minimizing the relative errors of measured flow stress and calculated value by the models. Therefore, an average standard deviation is proposed to evaluate the accuracy of the models. The average standard deviation is defined as

$$S = \frac{1}{n_1} \sum_{j=1}^{n_1} \sqrt{\sum_{i=1}^{m_1} (\sigma_{ij}^e - \sigma_{ij}^c)^2 / m_1} \quad (26)$$

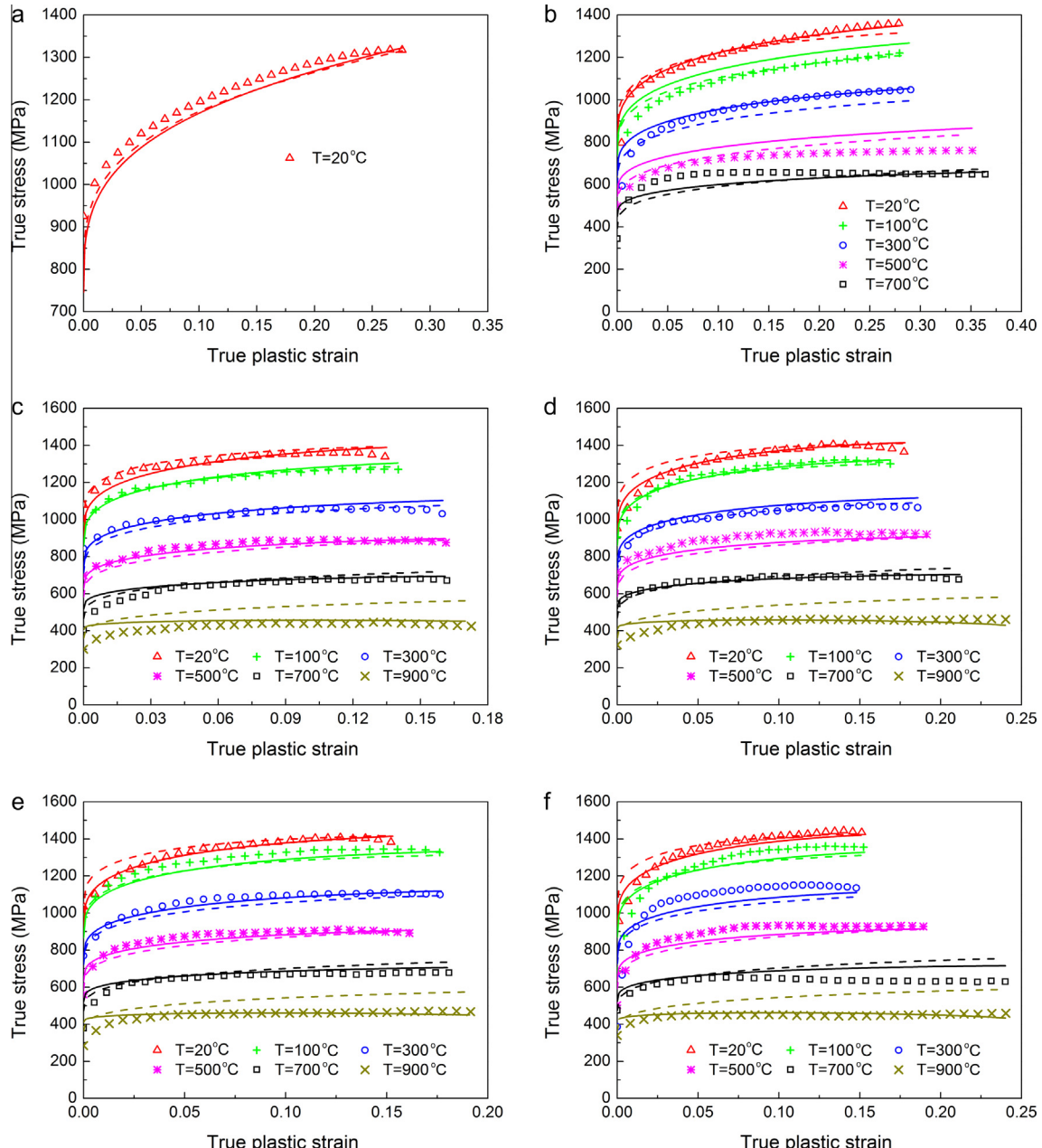
where  $n_1$  is the number of the test conditions, in this study  $n_1 = 30$  including the quasi-static and dynamic conditions;  $m_1 = 29$  is the number of the experimental points for each condition.  $\sigma_{ij}^e$  and  $\sigma_{ij}^c$  are the experimental and calculated flow stresses, respectively, at specific strain condition  $i$  and temperature condition  $j$ .

The average standard deviation represents the average distance of the calculated and measured flow stresses. The comparison of the average standard deviations of the four models is presented in Fig. 7. The average standard deviations of JC model and KHL model are approximately 55.6 MPa and 44.5 MPa, respectively, whereas the results of JCM and KHLM models are 42 MPa and 40.9 MPa, respectively. On the whole, the average standard deviations of the four models lie between 40.9 and 55.6 MPa. Meanwhile, as the measured flow stress for given conditions approximately lie between 400 MPa ( $T = 900^\circ\text{C}$ ) and 1200 MPa ( $T = 20^\circ\text{C}$ ), then the average standard deviation of the four models is 4–13% of the flow stresses. Therefore, the prediction accuracy of the four models can be acceptable for the flow stress modeling. In addition, to compare the precision of the models, the relative errors of the predicted and measured flow stresses at strain rate

**Table 2**

Optimized JC model parameters for Ti–6Al–4V alloy.

	<i>A</i> (MPa)	<i>B</i> (MPa)	<i>n</i>	<i>C</i>	<i>m</i>
Initial	796.57	818.113	0.291	0.026	0.66
Optimized	831.355	857.932	0.302	0.015	0.724

**Fig. 5.** Comparison of experimental flow stresses (symbols), JC model prediction (dash lines) and JCM models prediction (solid lines) for (a) 0.0001 s<sup>-1</sup>, (b) 0.01 s<sup>-1</sup>, (c) 2500 s<sup>-1</sup>, (d) 4000 s<sup>-1</sup>, (e) 7500 s<sup>-1</sup> and (f) 10,000 s<sup>-1</sup>.

of 10,000 s<sup>-1</sup>, with different strain and temperature conditions are calculated. The relative error of the flow stress is calculated as

$$\delta_{ij} = \left| \frac{\sigma_{ij}^e - \sigma_{ij}^c}{\sigma_{ij}^e} \right| \times 100\% \quad (27)$$

Fig. 8 presents the relative errors between the measured and predicted flow stresses using JC, JCM, KHL and KHLM models at 10,000 s<sup>-1</sup>. For the JC model, the relative error is smaller than 10%, except for the high temperature (700 °C and 900 °C) conditions. Besides, the relative error of JC model is independent on the

**Table 3**

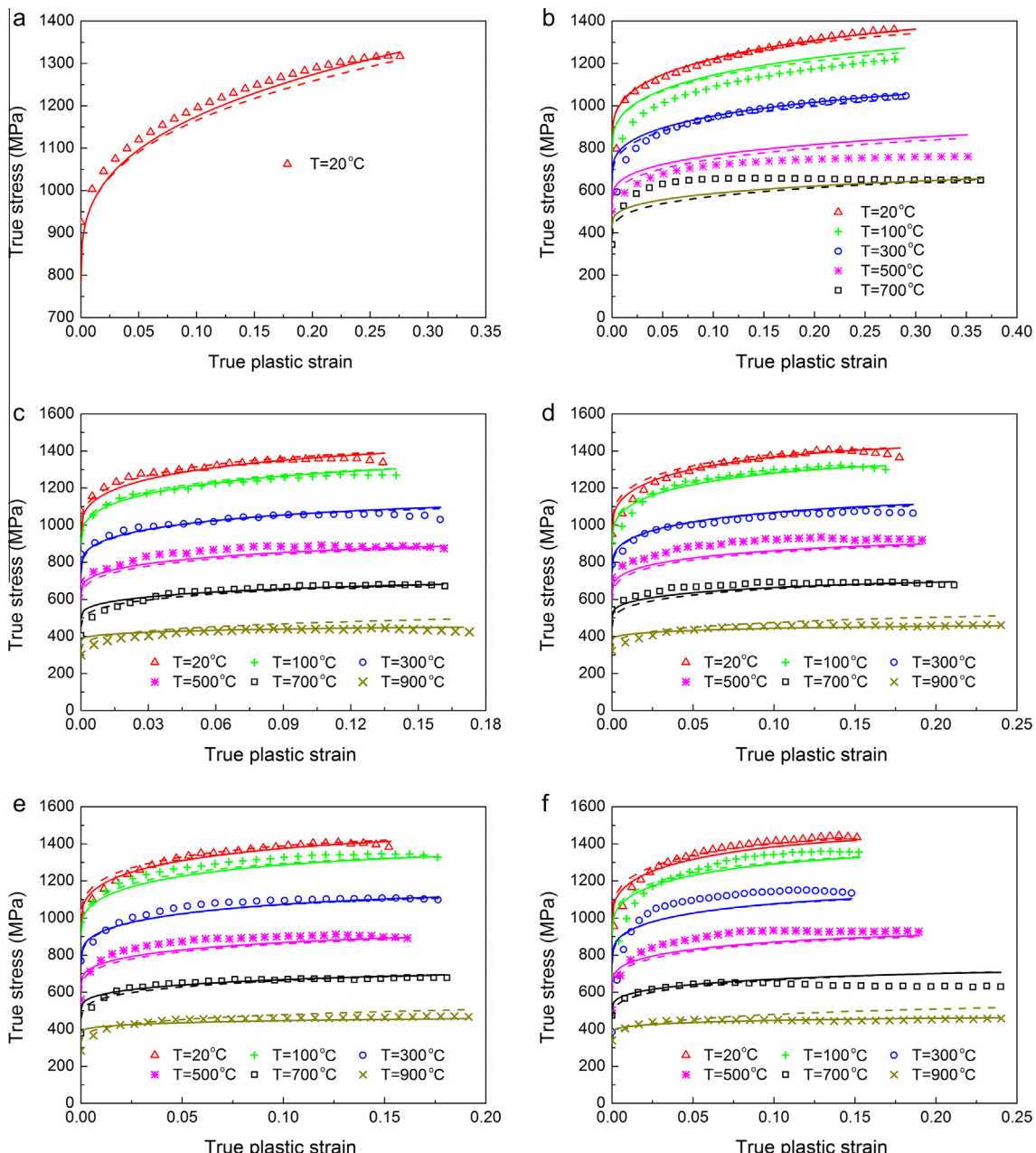
Optimized JCM model parameters for Ti–6Al–4V alloy.

	A (MPa)	B (MPa)	n	C	m	$n_2$	$T_0$ (°C)
Initial	796.57	800	0.291	0.026	0.735	0.396	500
Optimized	789.566	911.446	0.306	0.012	0.952	0.349	462.314

**Table 4**

Optimized KHL model parameters for Ti–6Al–4V alloy.

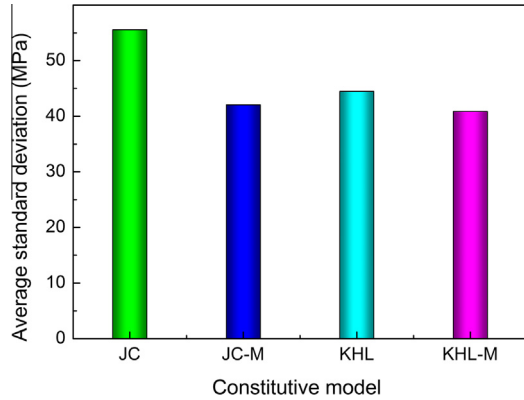
A (MPa)	B (MPa)	$n_1$	$n_0$	C	m
878.452	874.778	0	0.315	0.012	1.417

**Fig. 6.** Comparison of experimental flow stresses (symbols), KHL model prediction (dash lines) and KHLM models prediction (solid lines) for (a)  $0.0001 \text{ s}^{-1}$ , (b)  $0.01 \text{ s}^{-1}$ , (c)  $2500 \text{ s}^{-1}$ , (d)  $4000 \text{ s}^{-1}$ , (e)  $7500 \text{ s}^{-1}$  and (f)  $10,000 \text{ s}^{-1}$ .

**Table 5**

Optimized KHL model parameters for Ti-6Al-4V alloy.

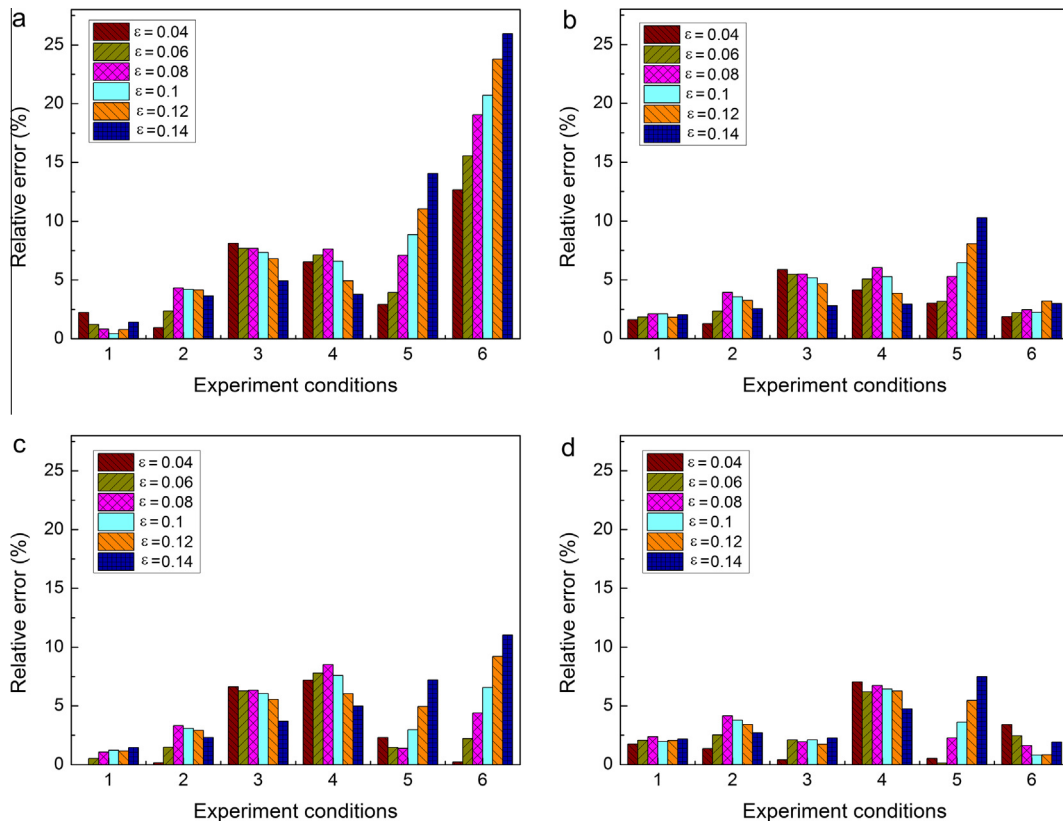
A (MPa)	B (MPa)	$n_1$	$n_0$	C	m	$n_2$	$T_0$ (°C)
872.791	906.428	0.012	0.327	0.011	1.211	0.214	456.453

**Fig. 7.** Comparison of the average standard deviations of the four constitutive models.

strain when  $T < 700$  °C, whereas the error increases with the strain at the condition of  $T = 700$  °C and  $T = 900$  °C, and it is mostly larger than 10%, even up to 25% at the strain of 0.12 and 0.14 when  $T = 900$  °C. That is, for the high strain rate condition ( $10,000\text{ s}^{-1}$ ), the JC model provides a good prediction for the flow stress, except

for the highest temperature. While, the relative errors of JCM model are smaller than the JC model, and most of the relative errors are less than 5%. Similarly, the relative errors of KHL model are less than 10%, while, most of the errors of KHL model are less than 5%, which exhibits high accuracy of prediction. In this work, the relative errors of other high strain rate conditions ( $2500\text{ s}^{-1}$ ,  $4000\text{ s}^{-1}$  and  $7500\text{ s}^{-1}$ ) are mostly less than that of  $10,000\text{ s}^{-1}$ , from the comparison of the flow stresses in Fig. 6c–e. Therefore, only the results at  $10,000\text{ s}^{-1}$  are discussed in this part to further illustrate the accuracy of the four models. The JCM and KHL model are better than the original JC and KHL model in modeling the flow stresses for Ti-6Al-4V alloy at the wide ranges of strain rate and temperature. That is, the temperature dependent work hardening constitutive models can provide more accurate prediction of the plastic deformation behavior than the original models.

From the comparison of the average standard deviation and the relative error of flow stresses, it can be concluded that the temperature item has a great influence on the strain rate hardening. To further examine the temperature effect on work hardening, the work hardening rates of the predicted flow stresses of the four models at  $7500\text{ s}^{-1}$  are calculated. According to Eq. (10), the work hardening rates of the JC, JCM, KHL and KHL-M models are defined as

**Fig. 8.** Variation of the relative errors of the (a. JC, b. JCM, c. KHL and d. KHL-M) models and experiment with strain and temperature: (1)  $10^4\text{ s}^{-1}$ , 20 °C, (2)  $10^4\text{ s}^{-1}$ , 100 °C, (3)  $10^4\text{ s}^{-1}$ , 300 °C, (4)  $10^4\text{ s}^{-1}$ , 500 °C, (5)  $10^4\text{ s}^{-1}$ , 700 °C and (6)  $10^4\text{ s}^{-1}$ , 900 °C.

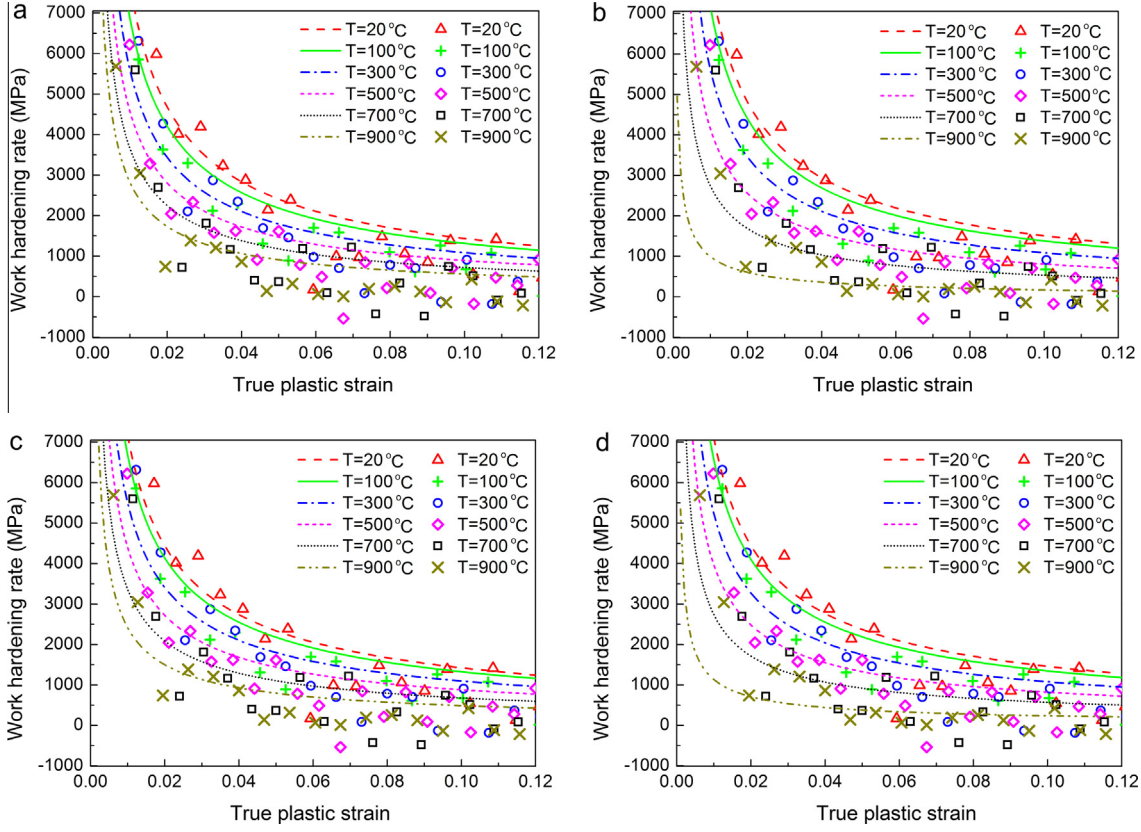


Fig. 9. The experimental and the (a. JC, b. JCM, c. KHL and d. KHLM) modeling work hardening rate at different temperatures (7500 s<sup>-1</sup>).

$$\left\{ \begin{array}{l} Q_{JC} = Bn(\dot{\varepsilon})^{(n-1)} \left[ 1 + C \ln \left( \frac{\dot{\varepsilon}}{\dot{\varepsilon}_0} \right) \right] \left[ 1 - \left( \frac{T-T_r}{T_m-T_r} \right)^m \right] \\ Q_{JCM} = Bn \left( \frac{T_0-T/2}{T_0} \right)^{n_2} (\dot{\varepsilon})^{(n-1)} \left[ 1 + C \ln \left( \frac{\dot{\varepsilon}}{\dot{\varepsilon}_0} \right) \right] \left[ 1 - \left( \frac{T-T_r}{T_m-T_r} \right)^m \right] \\ Q_{KHL} = Bn_0 \left( 1 - \frac{\ln \dot{\varepsilon}}{\ln D_0} \right)^{n_1} e^{(n_0-1)} \left( \frac{\dot{\varepsilon}}{\dot{\varepsilon}_0} \right)^C \left( \frac{T_m-T}{T_m-T_r} \right)^m \\ Q_{KHLM} = Bn_0 \left( 1 - \frac{\ln \dot{\varepsilon}}{\ln D_0} \right)^{n_1} \left( \frac{T_0-T/2}{T_0} \right)^{n_2} e^{(n_0-1)} \left( \frac{\dot{\varepsilon}}{\dot{\varepsilon}_0} \right)^C \left( \frac{T_m-T}{T_m-T_r} \right)^m \end{array} \right. \quad (28)$$

where  $Q_{JC}$ ,  $Q_{JCM}$ ,  $Q_{KHL}$  and  $Q_{KHLM}$ , are the work hardening rates of the JC, JCM, KHL and KHLM models, respectively.

Fig. 9a presents the comparison of the experimental and JC modeling work hardening rate at 7500 s<sup>-1</sup>. Both the experimental and modeling hardening rates decrease with the increasing plastic strain. That is in accordance with the exponential expression of the strain item. In addition, the experimental work hardening rate decreases with the increase of the temperature. Although the predicted hardening rate by JC constitutive equation exhibits a similar decreasing trend as experiment, due to the thermal softening item, the changing rate of the predicted hardening rate vs. temperature is smaller than that of experiment. While, in JCM model (as shown in Fig. 9b), the predicted changing rate of work hardening vs. temperature becomes larger. That is, the decrease of work hardening rate with the increase of temperature, or temperature dependent work hardening rate, is successfully correlated. Similarly, the work hardening rate of KHL model agrees with the experiment better than that of KHL model, as shown in Fig. 9c and d. That is, the introduced temperature dependent hardening item by Eq. (18) in the JCM and KHLM constitutive equations, rather than the thermal softening items, i.e.,  $1 - ((T - T_r)/(T_m - T_r))^m$  in JC equation and  $((T_m - T)/(T_m - T_r))^m$  in KHL equation, can describe the decrease of work hardening with the increasing temperature from 20 °C to 900 °C accurately. Besides, the comparison of the work hardening rates illustrates that the higher temperature curves are more

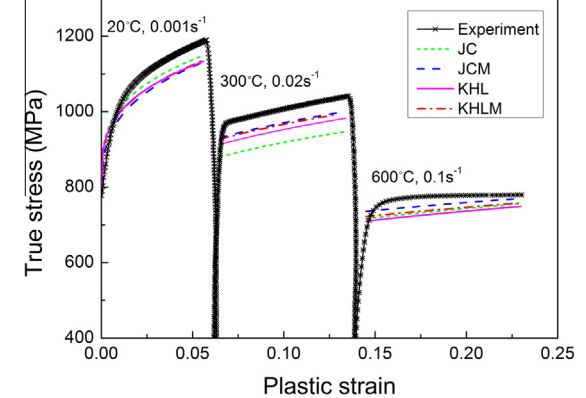


Fig. 10. Comparison of the experimental and predicted flow stresses at strain rate and temperature jump tests.

'square' in their representation, especially for 900 °C. That is, with the increase of temperature, the hardening rate becomes more stable in deformation process. For example, at 7500 s<sup>-1</sup>, 900 °C (Fig. 9d), both of the measured and calculated work hardening rates are more stable when the strain is larger than 0.02. Therefore, the flow stresses at 7500 s<sup>-1</sup>, 900 °C should exhibits a more stable flow stresses with the increase of plastic strain. The comparison of flow stresses at 900 °C (Fig. 6e) proves this conclusion, and this stable strain rate hardening at higher temperature can be caused by the microstructure evolution (e.g., dynamic recovery), due to the increase of the ductility as discussed in Section 2.4.

The experimental work hardening rate was calculated to validate the models under dynamic conditions. In addition, a strain rate as well as temperature jump test at quasi-static conditions were carried out to further validate the proposed models. Besides

the capability of characterizing the compression test experimental data, the effectiveness of a constitutive model is also dependent on its prediction accuracy for new conditions that are not determined experimentally [40]. Then the specimen was compressed at given new conditions considering the loading history: the specimen ( $\Phi 5 \times 4$  mm) was compressed until a plastic strain 0.056 at 20 °C and 0.001 s<sup>-1</sup>; afterwards, the loading condition was changed as 300 °C and 0.02 s<sup>-1</sup>, and the deformed specimen was sequentially compressed by strain 0.134; finally, the condition was changed as 600 °C and 0.1 s<sup>-1</sup>, and then was strain by 0.23. The sample was compressed from low to high temperature sequentially in order to eliminate the temperature effect on the microstructure of the material.

The measured flow stresses and the predicted results of the four models are shown in Fig. 10. For the three loading steps, the measured flow stresses is higher than the predicted results, however, most models can give a good prediction. For the first loading step, the predicted results of the models are close to each other, and the maximal error is about 5%; at the second step, the JC model give a less prediction than other models; at the third step, the predicted results are also close with each other. Besides, at 300 °C and 600 °C conditions, the JCM and KHL predicted results are closer to experimental results, and most of the relative errors are less than 5%.

## 5. Summary

In this work, an investigation was performed to explore the plastic deformation behavior of Ti-6Al-4V alloy by experiments and constitutive modeling, over a wide range of strain rates ( $10^{-4}$ – $10^4$  s<sup>-1</sup>) and temperatures (20–900 °C). The work hardening rates of the measured flow stresses under different strain rates were calculated. It was found that the work hardening rate is dependent on the temperature, at both the quasi-static and dynamic conditions. The deformed specimen and the microstructure exhibit different deformation mechanism at low (<500 °C) and high temperature (>500 °C) conditions. Material generates larger plastic deformation due to higher ductility and formability in high temperature deformation, which leads to decrease of work hardening rate. To characterize the plastic deformation behavior, the flow stresses under wide range of strain rates and temperatures were modeled with four constitutive models, i.e., the JC, JCM, KHL and KHLM models. Compared with the JC and KHL models, a temperature dependent work hardening item was introduced into the JCM and KHLM models. The parameters of the four models were obtained by a GA optimization method. From the comparison of the measured and predicted flow stresses, it was found that the average standard deviation of the models lies between 40.9 and 55.6 MPa. The average standard deviation of the four models is 4–13% of the flow stresses. On the whole, the four models can be considered as acceptable for predicting the plastic deformation behavior for Ti-6Al-4V alloy over the wide range of loading conditions.

In addition, based on the comparison of flow stresses at dynamic (10,000 s<sup>-1</sup>), the work hardening rates at dynamic (7500 s<sup>-1</sup>) as well as quasi-static jump experiments, the JCM model and KHLM models can characterize the temperature dependent work hardening effect accurately for Ti-6Al-4V alloy, over the wide range of deformation condition, involving the temperature scope of machining and hot working.

## Acknowledgments

The authors are very grateful for the support received from the Natural Science Foundation of China No. 51205284, Seed Foundation of Tianjin University and the Open Fund of Tianjin

Key Laboratory of Equipment Design and Manufacturing Technology. The authors would like to thank Prof. Guo Wei-Guo of Northwestern Polytechnical University for supplying the experimental equipment of the split Hopkinson bar tests.

## References

- [1] M.E. Nixon, O. Cazacu, R.A. Lebensohn, Anisotropic response of high-purity  $\alpha$ -titanium: experimental characterization and constitutive modeling, *Int. J. Plast.* 26 (4) (2010) 516–532.
- [2] L. Christoph, P. Manfred, *Titanium and Titanium Alloys: Fundamentals and Applications*, WILEY-VCH Verlag, 2003.
- [3] S. Nemat-Nasser, W.G. Guo, V.F. Nesterenko, S.S. Indrakanti, Y.B. Gu, Dynamic response of conventional and hot isostatically pressed Ti-6Al-4V alloys: experiments and modeling, *Mech. Mater.* 33 (8) (2001) 425–439.
- [4] C.W. James, G. Lutjering, *Titanium*, Springer-Verlag, 2003.
- [5] B. Babu, L.E. Lindgren, Dislocation density based model for plastic deformation and globularization of Ti-6Al-4V, *Int. J. Plast.* 50 (2013) 94–108.
- [6] W.S. Lee, C.F. Lin, Plastic deformation and fracture behaviour of Ti-6Al-4V alloy loaded with high strain rate under various temperatures, *Mater. Sci. Eng., A* 241 (1) (1998) 48–59.
- [7] A.S. Khan, Y. Sung Suh, R. Kazmi, Quasi-static and dynamic loading responses and constitutive modeling of titanium alloys, *Int. J. Plast.* 20 (12) (2004) 2233–2248.
- [8] A.S. Khan, R. Kazmi, B. Farrokh, M. Zupan, Effect of oxygen content and microstructure on the thermo-mechanical response of three Ti-6Al-4V alloys: experiments and modeling over a wide range of strain-rates and temperatures, *Int. J. Plast.* 23 (7) (2007) 1105–1125.
- [9] A. Molinari, C. Musquar, G. Sutter, Adiabatic shear banding in high speed machining of Ti-6Al-4V: experiments and modeling, *Int. J. Plast.* 18 (4) (2002) 443–459.
- [10] G. Chen, C.Z. Ren, X.Y. Yang, X.M. Jin, T. Guo, Finite element simulation of high speed machining of titanium alloy (Ti-6Al-4V) based on ductile failure model, *Int. J. Adv. Manuf. Technol.* 56 (9) (2011) 1027–1038.
- [11] G.G. Ye, S.F. Xue, M.Q. Jiang, X.H. Tong, L.H. Dai, Modeling periodic adiabatic shear band evolution during high speed machining Ti-6Al-4V alloy, *Int. J. Plast.* 40 (2013) 39–55.
- [12] H. Wu, S. To, Serrated chip formation and their adiabatic analysis by using the constitutive model of titanium alloy in high speed cutting, *J. Alloys Compd.* 629 (2015) 368–373.
- [13] G.R. Johnson, W.H. Cook, A constitutive model and data for metals subjected to large strains, high strain rates and high temperatures, in: Proceedings of the 7th International Symposium on Ballistics, vol. 21, 1983, pp. 541–547.
- [14] S. Seo, O. Min, H. Yang, Constitutive equation for Ti-6Al-4V at high temperatures measured using the SHPB technique, *Int. J. Impact Eng.* 31 (6) (2005) 735–754.
- [15] J.H. Sung, J.H. Kim, R.H. Wagoner, A plastic constitutive equation incorporating strain, strain-rate, and temperature, *Int. J. Plast.* 26 (12) (2010) 1746–1771.
- [16] D. Steglich, W. Brocks, J. Bohlen, F. Barlat, Modelling direction-dependent hardening in magnesium sheet forming simulations, *Int. J. Mater. Form.* 4 (2) (2011) 243–253.
- [17] A.S. Khan, S. Huang, Experimental and theoretical study of mechanical behavior of 1100 aluminum in the strain rate range  $10^{-5}$ – $10^4$  s<sup>-1</sup>, *Int. J. Plast.* 8 (4) (1992) 397–424.
- [18] A.S. Khan, S. Yu, Deformation induced anisotropic responses of Ti-6Al-4V alloy. Part I: experiments, *Int. J. Plast.* 38 (2012) 1–13.
- [19] U.F. Kocks, J.J. Jonas, H. Mecking, The development of strain-rate gradients, *Acta Metall.* 27 (3) (1979) 419–432.
- [20] F.J. Zerilli, R.W. Armstrong, Dislocation mechanics based constitutive relations for material dynamics calculations, *J. Appl. Phys.* 61 (5) (1987) 1816–1825.
- [21] S. Nemat-Nasser, Y. Li, Flow stress of fcc polycrystals with application to OFHC Cu, *Acta Mater.* 46 (2) (1998) 565–577.
- [22] A. Dutta, A. Vanderklok, S.A. Tekalur, High strain rate mechanical behavior of seashell-mimetic composites: analytical model formulation and validation, *Mech. Mater.* 55 (2012) 102–111.
- [23] A.S. Khan, M. Baig, Anisotropic responses, constitutive modeling and the effects of strain-rate and temperature on the formability of an aluminum alloy, *Int. J. Plast.* 27 (4) (2011) 522–538.
- [24] H. Mecking, U.F. Kocks, Kinetics of flow and strain-hardening, *Acta Metall.* 29 (11) (1981) 1865–1875.
- [25] P.S. Follansbee, G.T. Gray, An analysis of the low temperature, low and high strain-rate deformation of Ti-6Al-4V, *Metall. Trans. A* 20 (5) (1989) 863–874.
- [26] J. Luo, M. Li, X. Li, Y. Shi, Constitutive model for high temperature deformation of titanium alloys using internal state variables, *Mech. Mater.* 42 (2) (2010) 157–165.
- [27] Q. Zhao, G. Wu, W. Sha, Deformation of titanium alloy Ti-6Al-4V under dynamic compression, *Comput. Mater. Sci.* 50 (2) (2010) 516–526.
- [28] S.L. Semiatin, V. Seetharaman, I. Weiss, Flow behavior and globularization kinetics during hot working of Ti-6Al-4V with a colony alpha microstructure, *Mater. Sci. Eng., A* 263 (2) (1999) 257–271.
- [29] J. Porntadawit, V. Uthaisangsuk, P. Choungthong, Modeling of flow behavior of Ti-6Al-4V alloy at elevated temperatures, *Mater. Sci. Eng., A* 599 (2014) 212–222.

- [30] R.C. Picu, G. Vincze, F. Ozturk, J.J. Gracio, F. Barlat, A.M. Maniatty, Strain rate sensitivity of the commercial aluminum alloy AA5182-O, *Mater. Sci. Eng., A* 390 (1) (2005) 334–343.
- [31] B. Berisha, P. Hora, A. Wahlen, L. Tong, A combined isotropic-kinematic hardening model for the simulation of warm forming and subsequent loading at room temperature, *Int. J. Plast.* 26 (1) (2010) 126–140.
- [32] D. Yu, X. Chen, W. Yu, G. Chen, Thermo-viscoplastic modeling incorporating dynamic strain aging effect on the uniaxial behavior of Z2CND18, 12N stainless steel, *Int. J. Plast.* 37 (2012) 119–139.
- [33] F. Kabirian, A.S. Khan, A. Pandey, Negative to positive strain rate sensitivity in 5xxx series aluminum alloys: experiment and constitutive modeling, *Int. J. Plast.* 55 (2014) 232–246.
- [34] B. Farrokh, A.S. Khan, Grain size, strain rate, and temperature dependence of flow stress in ultra-fine grained and nanocrystalline Cu and Al: synthesis, experiment, and constitutive modeling, *Int. J. Plast.* 25 (5) (2009) 715–732.
- [35] J.S. Tiley, Modeling of Microstructure Property Relationships in Ti-6Al-4V, Ph.D. thesis, Ohio State University, 2002.
- [36] T. Seshacharyulu, S.C. Medeiros, W.G. Frazier, Y.V.R.K. Prasad, Microstructural mechanisms during hot working of commercial grade Ti-6Al-4V with lamellar starting structure, *Mater. Sci. Eng., A* 325 (2002) 112–125.
- [37] Y. Xi, M. Bermingham, G. Wang, M. Dargusch, SPH/FE modeling of cutting force and chip formation during thermally assisted machining of Ti6Al4V alloy, *Comput. Mater. Sci.* 84 (2014) 188–197.
- [38] S. Nemat-Nasser, J.B. Isaacs, Direct measurement of isothermal flow stress of metals at elevated temperatures and high strain rates with application to Ta and Ta-W alloy, *Acta Mater.* 45 (3) (1997) 907–919.
- [39] J.J. Wang, W.G. Guo, X.S. Gao, J. Sun, The third-type of strain aging and the constitutive modeling of a Q235B steel over a wide range of temperatures and strain rates, *Int. J. Plast.* 65 (2015) 85–107.
- [40] Z. Xu, F. Huang, Thermomechanical behavior and constitutive modeling of tungsten-based composite over wide temperature and strain rate ranges, *Int. J. Plast.* 40 (2013) 163–184.
- [41] J. Zhang, H. Di, X. Wang, Y. Cao, J. Zhang, T. Ma, Constitutive analysis of the hot deformation behavior of Fe–23Mn–2Al–0.2C twinning induced plasticity steel in consideration of strain, *Mater. Des.* 44 (2013) 354–364.
- [42] M.C. Mataya, V.E. Sackschewsky, Effect of internal heating during hot compression on the stress-strain behavior of alloy 304L, *Metall. Mater. Trans. A* 25 (12) (1994) 2737–2752.
- [43] Military Handbook, Metallic materials and elements for aerospace vehicle structures, MIL-HDBK-5H, DOD and FAA, 1998.
- [44] J. Peirs, W. Tirry, B. Amin-Ahmadi, Microstructure of adiabatic shear bands in Ti6Al4V, *Mater. Charact.* 75 (2013) 79–92.
- [45] X.P. Zhang, R. Shrivpuri, A.K. Srivastava, Role of phase transformation in chip segmentation during high speed machining of dual phase titanium alloys, *J. Mater. Process. Technol.* 214 (2014) 3048–3066.
- [46] S. Joshi, P. Pawar, A. Tewari, Influence of  $\beta$  phase fraction on deformation of grains in and around shear bands in machining of titanium alloys, *Mater. Sci. Eng., A* 618 (2014) 71–85.
- [47] J. Schneider, L. Dong, J.Y. Howe, I.I.H.M. Meyer, Microstructural characterization of Ti-6Al-4V metal chips by focused ion beam and transmission electron microscopy, *Metall. Mater. Trans. A* 42 (11) (2011) 3527–3533.
- [48] G. Chen, C. Ren, W. Yu, X. Yang, L. Zhang, Application of genetic algorithms for optimizing the Johnson–Cook constitutive model parameters when simulating the titanium alloy Ti-6Al-4V machining process, *Proc. Inst. Mech. Eng. Part B: J. Eng. Manuf.* 226 (8) (2012) 1287–1297.